

Does magnetic pressure affect the ICM dynamics?

D. R. Gonçalves^{1,2} and A. C. S. Friaça¹

¹ *Instituto Astronômico e Geofísico - USP, Av. Miguel Stefano 4200, 04301-904 São Paulo, SP, Brazil*

² *Instituto de Astrofísica de Canarias, E-38200 La Laguna, Tenerife, Spain*

denise@ll.iac.es, amancio@iagusp.usp.br

ABSTRACT

A possible discrepancy found in the determination of mass from gravitational lensing data, and from X-rays observations, has been largely discussed in the latest years. For instance, Miralda-Escudé & Babul (1995) have found that the mass estimate derived from gravitational lensing can be as much as a factor of 2–2.5 larger than the mass estimate derived from analysis of the X-rays observations. Another important discrepancy related to these data is that X-ray imaging, with some spectral resolution, suggest that the mass distribution of the gravitating matter, mostly dark matter, has a central cusp, or at least that the dark matter is more centrally condensed than the X-ray-emitting gas, and also with respect to the galaxy distribution (Eyles et al. 1991), at variance to what is expected from the most accepted models of formation of large scale structure. Could these discrepancies be consequence of the standard description of the ICM, in which it is assumed hydrostatic equilibrium maintained by thermal pressure? In analogy to the interstellar medium of the Galaxy, it is expected a non-thermal term of pressure, which contains contributions of magnetic fields, turbulence and cosmic rays. We follow the evolution of the ICM, considering a term of magnetic pressure, aiming at answering the question whether or not these discrepancies can be explained via non-thermal terms of pressure. Our results suggest that the magnetic pressure could only affect the dynamics of the ICM on scales as small as $\lesssim 1$ kpc. Our models are constrained by the observations of large and small scale fields and we are successful at reproducing available data, for both Faraday rotation limits and inverse Compton limits for the magnetic fields. In our calculations the radius (from the cluster center) in which magnetic pressure reaches equipartition is smaller than radii derived in previous works. The crucial difference in our models comes from our more realistic treatment of the magnetic field geometry, and from the consideration of a sink term in the cooling flow which reduces the amplification of the field strength during the inflow. In addition the magnetic field calculations are changed after the cooling flow has been formed.

Key words: Galaxies: clusters – Intracluster medium – Cooling flows – X-rays: galaxies – Gravitational lensing – Magnetic fields

1 INTRODUCTION

Since the work of Loeb & Mao (1994), the possibility of explaining the discrepancies on mass determinations, found by Miralda-Escudé & Babul (1995), via non-thermal pressure support has been widely discussed (see also Wu & Fang 1996, 1997; Wu et al. 1998). The discrepancy arises from the two most promising techniques to obtain clusters of galaxies masses. On one hand, the determination of masses in clusters of galaxies, via X-ray data, is based on the hypothesis that the ICM is in hydrostatic equilibrium with the gravitational potential, using the radial profiles of density and temperature. There are uncertainties in the determination of temperature profiles, particularly for radii > 1 Mpc, and for

most systems only a mean emission-weighted X-ray temperature is available (radial temperature profiles are available only for a few clusters ,e.g., Allen & Fabian 1994; Nulsen & Böhringer 1995). On the other hand, gravitational lensing measures the projected surface density of matter, a method which makes no assumptions on the dynamical state of the gravitating matter (Fort & Mellier 1994; Miralda-Escudé & Babul 1995; Smail et al. 1997).

One can find in the literature some attempts to resolve the discrepancy between X-ray and gravitational lensing mass measurements of clusters of galaxies. For instance, Allen (1998) studied in detail a sample of 13 galaxy clusters (including cooling flows, intermediate and non-cooling flows systems) with the goal of comparing X-ray and lensing mass

arXiv:astro-ph/9906453v2 8 Jul 1999

measurements. His conclusions pointed out that, at least for cooling flows systems, being more relaxed systems, this discrepancy is completely resolved, and therefore, non-thermal pressures can be discarded in these systems.

The magnetic field of the ICM can be obtained via Faraday rotation, due to the effect of magnetic field on the polarized radio emission from the cluster or the background radio sources. The polarization plane of linearly polarized radiation is rotated during the passage through a magnetized plasma. The angle of rotation is $\phi = (RM)\lambda^2$, where RM is the rotation measure and λ the radiation wavelength (Sarazin 1992, for a review). In clusters with diffuse radio emission, X-ray observations can give a lower limit to the strength of the magnetic field. Typically, this limit is $B \geq 0.1 \mu\text{G}$ (Rephaeli et al. 1987) on scales of ~ 1 Mpc. In the case of Faraday rotation the information obtained is the upper limit on the intensity of the field, and the measured values are $RM \leq 100 \text{ rad/m}^2$, that is more or less consistent with an intracluster field of $B \sim 1 \mu\text{G}$, with a coherence length of $l_B \leq 10$ kpc. This strength of the magnetic field corresponds to a ratio of magnetic to gas pressure of $p_B/p_{gas} \leq 10^{-3}$, implying that B does not influence the cluster dynamics (at least on large scales).

At inner regions, of the cooling flow clusters, the magnetic fields are expected to be amplified due to the gas compression (Soker & Sarazin 1990). If they are frozen in the mass flow flux, and if this flux is homogeneous and spherically symmetric, $B \propto r^{-1}$ and $RM \propto r^{-1}$, ($p_B \propto r^{-2}$ and the gas pressure increases slowly). Even in this case p_B reaches equipartition at a radius r_B of $r_B \sim 1 \text{ kpc} \left(\frac{B}{1 \mu\text{G}}\right)^{1/2} \left(\frac{M}{100 M_\odot \text{ yr}^{-1}}\right)^{1/3}$. In these inner regions many sources with very strong Faraday rotations were observed, in which the rotation measure can reach values of $RM \sim 4000 \text{ rad/m}^2$ (radio sources associated with the central galaxies of the clusters with very strong cooling flows (M87/Virgo, Cyg A, Hydra A, 3C 295, A1795)), implying, $B \geq 10 \mu\text{G}$ at $l_B \sim 1$ kpc (Taylor & Perley 1993; Ge & Owen 1993, 1994). These observations strongly suggest that the Faraday rotation is created by magnetic fields within the cooling flow clusters.

Another promising method to estimate the cluster scale magnetic field, as cited above, is the detection of co-spatial inverse Compton X-ray emission with the synchrotron plasma emission (the 3 K background photons scattering off the relativistic electrons can produce a diffuse X-ray emission) (Rephaeli & Gruber 1988). Therefore, this method provides limits on the cluster scale magnetic fields, in addition of limits on the non-thermal amount of X-ray emission (or even on the relativistic electrons energy) in galaxy clusters. Such a kind of detection of clusters magnetic fields leads, using ROSAT PSPC data and also 327 MHz radio map of Abell 85 (a cooling flow cluster, with a central dominant cD galaxy and about $100 M_\odot/\text{yr}$), to an estimate of $(0.95 \pm 0.10) \mu\text{G}$ (Bagchi et al. 1998). However, even non-cooling flows clusters present this diffuse, relic radio source which can be used to estimate magnetic field strength. For instance Ensslin & Biermann (1998) studied limits on the Coma cluster magnetic field strength, using this multifrequency observations. They shown that the central magnetic field limit is $B > 0.3 \mu\text{G}$. Others have determined the strength of the magnetic field for Coma cluster, using dif-

ferent techniques and obtaining similar values: $B \leq 1.2 \mu\text{G}$ (Lieu et al. 1996); $B > 0.4 \mu\text{G}$ (Sreekumar et al. 1996). For the same cluster (Coma), but using Faraday rotation measure, Feretti et al. (1995) estimated magnetic fields of $6.0 \mu\text{G}$ (at scales of 1 kpc), and of $1.7 \mu\text{G}$ (at scales of 10 kpc) was estimated by Kim et al. (1990).

The above scenario allow us conclude that for both methods the observational resolution of the telescope limits the detection of smaller scales magnetic fields, implying that at scales smaller than 1 kpc the magnetic field strength can be higher (Ensslin et al. 1997). Another point to be noted is that Faraday rotation measures always gives values higher than inverse Compton/CBM measures. Anyway, these fields are present in the ICM and therefore justify the such a kind of study we present here. Other theoretical works concerning the magnetic pressure on the ICM are available (for instance Soker & Sarazin 1990; Tribble 1993; Zoabi et al. 1996) and we briefly compare our results with those obtained by these authors.

Our goal in this paper is trying to answer the question whether or not magnetic support can be relevant in cooling flow clusters, using a more realistic treatment of the magnetic field geometric evolution. The scope of the paper is the following: in Section 2 we present the hydrodynamical equations and the method applied for their solution; Section 3 describes our models and results compared to the available observations; and in Section 4 we discuss our results in the light of others obtained in previous works, as well our main conclusions.

2 EVOLUTION OF THE ICM WITH MAGNETIC PRESSURE

The evolution of the intracluster gas is obtained by solving the hydrodynamic equations of mass, momentum and energy conservation:

$$\frac{\partial \rho}{\partial t} + \frac{1}{r^2} \frac{\partial}{\partial r} (r^2 \rho u) = -\omega \rho \quad (1)$$

$$\frac{\partial u}{\partial t} + u \frac{\partial u}{\partial r} = -\frac{1}{\rho} \frac{\partial p_t}{\partial r} - \frac{GM(r)}{r^2} \quad (2)$$

$$\frac{\partial U}{\partial t} + u \frac{\partial U}{\partial r} = \frac{p_t}{\rho^2} \left(\frac{\partial \rho}{\partial t} + u \frac{\partial \rho}{\partial r} \right) - \Lambda \rho \quad (3)$$

where u , ρ , p_t , U are the gas velocity, density, total pressure and the specific internal energy. The equation of state relates U and the temperature,

$$U = \frac{3}{2} \frac{k_B T}{\mu m_H} \quad (4)$$

(k_B is the Boltzmann's constant, m_H is the hydrogen atom mass and $\mu = 0.62$ is the mean molecular weight of a fully ionized gas with 10% helium by number). The mass distribution, $M(r)$, is due to the contribution of the X-rays emitting gas plus the cluster collisionless matter (which is the sum of the contributions of galaxies and dark matter – the latter being dominant), i.e., $M(r) = M_g(r) + M_{cl}(r)$. $M_{cl}(r)$ follows

$$\rho_{cl}(r) = \rho_0 \left(1 + \frac{r^2}{a^2} \right)^{-3/2} \quad (5)$$

in which ρ_0 and a (the cluster core radius) are related to σ (the line-of-sight velocity dispersion) via: $9\sigma^2 = 4\pi G a^2 \rho_0$.

The total pressure p_t is the sum of thermal and magnetic pressure, e.g., $p_t = p + p_B$. The constraints to the magnetic pressure come from observations, from which $p_B = B^2/8\pi \simeq 4 \times 10^{-14} \text{ erg cm}^{-3} \text{ s}^{-1}$ (cf. Bagchi et al. 1998) for a diffuse field located at $\sim 700h_{50}^{-1} \text{ kpc}$ from the cluster center. Along this paper we will use mostly the ratio between magnetic and thermal pressures, or the β -parameter, $\beta = p_B/p$.

The sink term $\omega\rho$ in the mass equation describes the removal of mass from the gas flow by thermal instabilities. The importance of the gas removal was studied in detail by Friaça (1993) following the q -description described by White & Sarazin (1987). The sink is particularly important when one searches for a steady state solution of the cooling flow without an implausible huge accumulation of mass at the center. In fact, the condensations formed by the sink will probably give rise to stars, planetary bodies or cold dense clouds which in turn will constitute a halo surrounding the central dominant galaxy. We assume isobaric removal, so that the sink does not introduce any additional term in the energy equation. Summing up the physics contained in this term one can say that the specific mass removal rate is $\omega = q/t_c$ where the denominator is the instantaneous isobaric cooling time, such that the removal efficiency q relates the cooling time to the growth time scale of the thermal instability in the cooling flow. We assume q between 1.0 and 1.5, which are the q -values found to be more consistent with the observations (Friaça 1993).

The cooling function adopted $\Lambda(T)$ is the cooling rate per unit volume. Since there is no ionization equilibrium for temperatures lower than 10^6 K , we adopt a non-equilibrium cooling function for the gas at $T < 10^6 \text{ K}$ (the recombination time of important ions is longer than the cooling time at these temperatures). The cooling function was calculated with the atomic database of the photoionization code AANGABA (Gruenwald & Viegas 1992). The adopted abundances are sub-solar as appropriate for the ICM (Edge & Stewart 1991; Fabian 1994; Grevesse & Anders 1989).

Despite the presence of steep temperature gradients we did not consider thermal conduction in our models. This can be justified using the fact that on a global scale cooling flow clusters contain cooler gas near the center and hotter gas further out. Therefore, the presence of cooling flows is itself a proof that thermal conduction effect is, at least, reduced in the ICM. Models show that thermal conduction would erase the observed density and temperature gradients in cooling flows, unless it is inhibited (see, for instance, Friaça 1986; David & Bregman 1989). It is well known that even weak magnetic field, if it is tangled, can inhibit the thermal conduction perpendicular to the field lines. More recently it has been argued that electromagnetic instabilities driven by temperature gradients (or electric currents in other situations) also can cause this inhibition in cooling flows (Pistinner et al. 1996), even for non-tangled field lines.

A spherically symmetric Eulerian code is employed for the calculations, which are solved via the finite-difference scheme based on Cloutman (1980). The grid points are spaced logarithmically, with a grid of 100 cells, with the first being 50 pc wide. The innermost cell edge is located at 100 pc and the outer boundary at twice the tidal radius

of the cluster. The artificial viscosity for the treatment of the shocks follows the formulation of Tscharnuter & Winkler (1979) based on the Navier-Stokes equation. The outer boundary conditions on pressure and density are derived by including an outer fictitious cell, the density and pressure in which are obtained from extrapolation of power laws over the radius fitted to the five outermost real cells. The inner boundary conditions are adjusted according to whether inflow (velocity at the inner boundary is extrapolated from the velocities at the innermost cell edges) or outflow (velocity is set zero) prevails locally. The initial conditions for the gas are an isothermal atmosphere ($T_0 = 10^7 \text{ K}$) with 30% solar abundances and density distribution following that of the cluster dark matter. The evolution is followed until the age of 14 Gyr.

The initial β value used here was derived from the magnetic field observations (using, for instance, Bagchi et al. 1998; Ge & Owen 1993, 1994; Ensslin & Biermann 1998; Ruy & Biermann 1998). We assume: frozen-in field; spherical symmetry for the flow and the cluster itself; and that at $r > r_c$ (the cooling radius, see below), the magnetic field is isotropic, i.e.,

$$B_r^2 = B_t^2/2 = B^2/3$$

and $l_r = l_t \equiv l$ (where B_r and B_t are the radial and transversal components of the magnetic field B and l_r and l_t are the coherence length of the large-scale field in the radial and transverse directions). In order to calculate B_r and B_t for $r < r_c$ we modified the calculation of the magnetic field of Soker & Sarazin (1990) by considering an inhomogeneous cooling flow (i.e. $M_i \neq \dot{M}$ varies with r). Therefore, the two components of the field are then given by

$$\frac{D}{Dt} (B_r^2 r^4 \dot{M}^{-2}) = 0$$

and

$$\frac{D}{Dt} (B_t^2 r^2 u^2 \dot{M}^{-1}) = 0.$$

In our models we take as reference radius the cooling radius r_c . In fact we modify the geometry of the field when and where the cooling time comes to be less than 10^{10} yr (usually adopted as the condition for the development of a cooling flow). Therefore, our condition to assume a non-isotropic field is $t_{c,oo} \equiv 3k_B T / 2\mu m_H \Lambda(T)\rho \leq 10^{10} \text{ yr}$. After the formation of the cooling flow, in the inner regions of the ICM, the magnetic field geometry is changed, following the enhancement of the radial component of the field, due to the enhancement of the density.

3 MODELS AND RESULTS

In this section we present the results of our models. There are four parameters to consider in each one of the models: σ , the cluster velocity dispersion; ρ_0 , the initial average mass density of the gas; a , the cluster core radius; and β_0 , the initial magnetic to thermal pressure ratio. We adopted the removal efficiency $q = 1.5$.

The most important results of our models are shown on figures we describe below, for which we assume: $\sigma = 1000 \text{ km s}^{-1}$ and $a = 250 \text{ kpc}$. First of all, the evolution we follow here is characteristic of cooling flow clusters and in

this scenario we discuss the evolution of the basic thermodynamics parameters. Considering the overall characteristics of our models, we will compare the results with the very recent study based on ROSAT observations of the cores of clusters of galaxies, by Peres et al. (1998), focusing on cooling flows in a X-rays flux-limited sample (containing the brightest 55 clusters over the sky in the 2–10 keV band). Comparing the present models with Peres et al. (1998) deprojection results, we see that the central cooling time here adopted as our cooling flow criterion, e.g. $t_{\text{cool}} \lesssim 10^{10}$ yr, is typical for a fraction between 70% and 90% of their sample. They also discuss briefly the cooling flow age, remembering that in hierarchical scenarios for the formation of structures in the Universe, clusters are formed by smaller substructures by mergers, and therefore the estimation of the cooling flows ages (and the cluster ages themselves) is complicated. Anyway they determine the fraction of cooling flow clusters in their sample considering a factor of two in the ages and concluding that the fraction do not vary that much (from 13 Gyr to 6 Gyr, the fraction varies from 70% to 65%). This allow us conclude that our models, which present cooling flows since the cluster has the age of $\sim 7 - 9$ Gyr, are typical for their sample. As a matter of fact, the time in which the cooling flow structure is formed depends strongly on the initial density we adopted. For models with $\rho_0 = 1.25 \times 10^{-28}$ g cm $^{-3}$ it rises on ~ 9 Gyr, while the models with $\rho_0 = 1.5 \times 10^{-28}$ g cm $^{-3}$ have it formed on ~ 7 Gyr. We will come back to this point later while analyzing the field anisotropy.

The characteristics of our models are summarized using four typical set of initial parameters, and discussing some details which came up of the study of a larger grid of parameters. Therefore, each model is characterized by its position in the (ρ_0, β_0) parameter space: model I ($\rho_0 = 1.5 \times 10^{-28}$ g cm $^{-3}$, $\beta_0 = 10^{-2}$); model II ($\rho_0 = 1.5 \times 10^{-28}$ g cm $^{-3}$, $\beta_0 = 10^{-3}$); model III ($\rho_0 = 1.25 \times 10^{-28}$ g cm $^{-3}$, $\beta_0 = 10^{-2}$); and model IV ($\rho_0 = 1.25 \times 10^{-28}$ g cm $^{-3}$, $\beta_0 = 10^{-3}$).

Figure 1 shows the evolution of density and temperature profiles corresponding to model I, from which the presence of the cooling flow on later stages of the ICM evolution and at inner regions is remarkable if one notices the steep gradients of these quantities. In order to better understand how the magnetic field geometry is modified after the cooling flow formation, e.g., after the steepness on the temperature and density gradients, we follow the evolution of the degree of anisotropy, using the concepts previously defined on Section 2, concerning the geometry of the magnetic field. Hereafter we called ‘degree of anisotropy’ the ratio B_t/B_r , noting that for the isotropic case it results $\sqrt{2}$ and the more anisotropic the field geometry the smaller is this ratio. Therefore, we present on Figure 2 the evolution of the degree of anisotropy since ~ 3.3 Gyr, comparing models I and III, in which one can see, clearly, that the anisotropy begins decreasing on earlier times for models with higher ρ_0 (model I) than for the ones with lower values of ρ_0 (model III). From Figure 2 we are allowed to conclude that the degree of anisotropy can be seen as a sensor of the presence of the cooling flow. In another words, the change in the degree of anisotropy can be used as another criterion to indicate the epoch, on the ICM evolution, in which the cooling flow appear.

These results can also be discussed in the light of some observational works in which the limits to the magnetic field

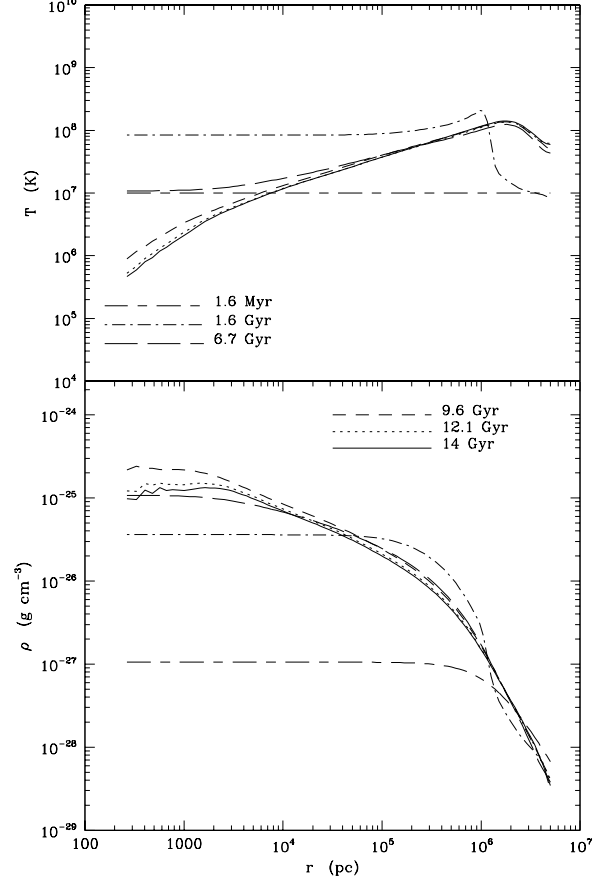


Figure 1. Evolution of the density and temperature profiles. Curves represent early and late stages of the ICM evolution, as labeled, for model I. Noting the steep gradients of these quantities, i.e., the presence of the cooling flow, at inner regions of the cluster, on later stages of the ICM evolution.

strength on large and small scales of the cooling flow clusters are given. Following such a kind of observations, as previously seen in the introduction section, we chose two values of magnetic field strength derived by the authors below. The first one is presented in Bagchi et al. (1998) who estimated, from inverse Compton X-ray emission with the synchrotron emission plasma, a cluster-scale (700 kpc) magnetic field strength of (0.95 ± 0.10) μG for Abell 85 (a cooling flow cluster with a central dominant cD galaxy and $\dot{M} \simeq 100$ M_{\odot}/yr). The second one is presented in two papers of Ge & Owen (1993, 1994), in which they present and discuss rotation measures and the related intensity of the magnetic field, giving a range of this intensity at scales of 10 kpc. Therefore, our results for the magnetic field strength and also for pressures, on large and small scales, are compared to the chosen observed ones, in Figures 3 and 4. Reminding that the time on which the cooling flow arises is closely related to ρ_0 , one can expect distinct results on the evolution of the field intensity from, for instance, model I to model III. However this evolution can be better explained comparing model I (Figure 3) to model II (Figure 4), since these two models have the same initial density but distinct β_0 .

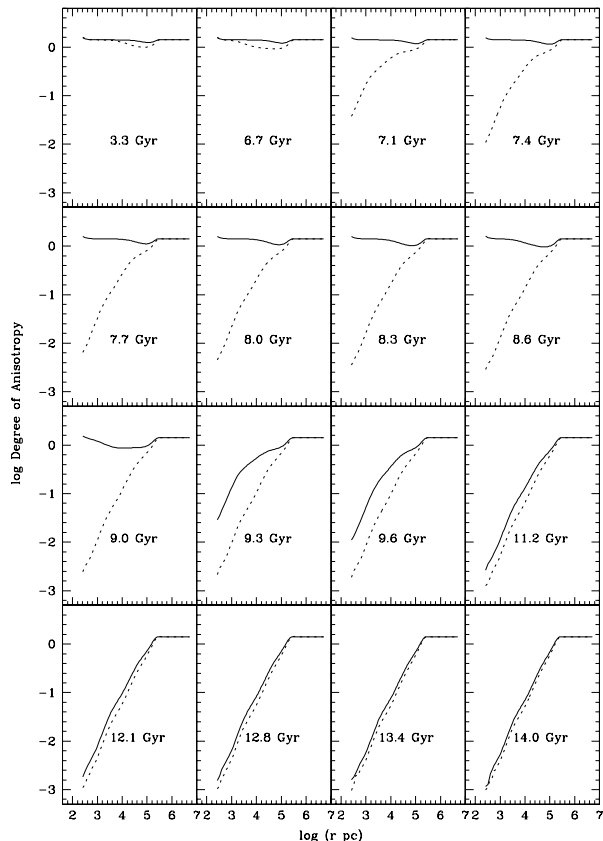


Figure 2. Evolution of the anisotropy degree, the tangential to radial magnetic field components ratio, for model I (dashed lines) and III (full lines), on late stages of the ICM evolution. Noting that the presence of the cooling flow, at inner regions, $\lesssim 200$ kpc, and on late stages, $\gtrsim 9.6$ Gyr, of the ICM evolution (see Figure 1) matches very well with the decrease of the anisotropy degree, and that it occurs earlier for model I.

Our best model, in terms of the magnetic field strength compared with observations, is model I ($\rho_0 = 1.5 \times 10^{-28} \text{ g cm}^{-3}$, $\beta_0 = 10^{-2}$). From Figure 3 it is possible to see that on scales of 700 kpc the magnetic field expected for the model is higher than the observed one (considering, of course, the profile correspondent to redshift zero, or evolution times on the order of 13 – 14 Gyr), while on scales of 10 kpc the model gives a value lower than the observed one. Meanwhile, at least on scales of 700 kpc, the situation is inverted if one takes a look on Figure 4, for which $\rho_0 = 1.5 \times 10^{-28} \text{ g cm}^{-3}$, but $\beta_0 = 10^{-3}$. Given the uncertainties characteristics of the observations, we can say that our models are in agreement with the magnetic field estimations available.

On Figures 5 and 6 we show the magnetic and thermal pressures evolution, or in another words, β -evolution, for models I and II respectively, on later times of the ICM evolution, in order to analyze when and where magnetic pressure reaches equipartition. Obviously the magnetic pressure is compatible with the magnetic field intensities and may be compared to the values determined by, for instance, Bagchi et al. (1998), $p_B = B^2/8\pi \simeq 4 \times 10^{-14} \text{ erg cm}^{-3} \text{ s}^{-1}$, at

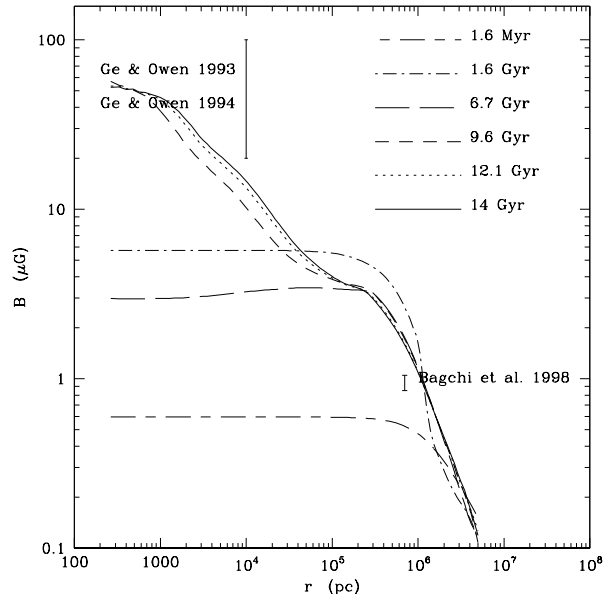


Figure 3. Evolution of the magnetic strength profiles compared to the observations. Curves represent early and late stages of the ICM evolution, as labeled, for model I ($\rho_0 = 1.5 \times 10^{-28} \text{ g cm}^{-3}$; $\beta_0 = 10^{-2}$). Note that the intensity B of the magnetic field at 6.7 Gyr is smaller than at 1.6 Gyr, due to the fact that at 6.7 Gyr the ICM is in the verge of developing a cooling flow, as we can see from the drop in temperature in the central region, as shown in Figure 1. In the evolution of the ICM before the onset of the cooling flow, the magnetic pressure keeps track of the thermal pressure, following the initial conditions for $p_B/p = \beta_0 < 1$, and the reduction in the thermal pressure just after the onset of the cooling flow is reflected in the evolution of B . Only after the cooling flow has been established, leading to amplification of B , the intensity of the magnetic field will rise to high values.

scales of 700 kpc, on the present time. From the analysis of the magnetic pressures expected from our models it is clear that they agree, as well as the magnetic field strength, with the observations. Here again model I appears being the best one, with ($\beta_0 = 10^{-2}$), but the values expected from model II are not far away from the observed ones as well. Noting also that magnetic pressure and/or magnetic intensity does not change very much after 12 Gyr, for both cases. Results presented on Figures 3 - 6 would indicate that we should adopt an intermediate initial value for β (like $\beta_0 = 5 \times 10^{-3}$) in order to obtain a magnetic field intensity in better agreement with the observations, at least on scales of 700 kpc. Nevertheless such an exercise should not solve the match of models and observations on smaller scales, since $\beta_0 \simeq 5 \times 10^{-3}$ should decrease magnetic pressure on scales of 10 kpc, at the present time, as a result of the present modelling assumptions (see Figure 4).

Other proposals for the amplification of the magnetic field in the center of the cooling flow clusters are: i) rotational driven mechanisms, in which the twisting of the magnetic flux tubes and/or the operation of fast $\alpha - \omega$ dynamo are the responsible for the increase of the magnetic strength (Godon et al. 1998); ii) turbulence induced am-

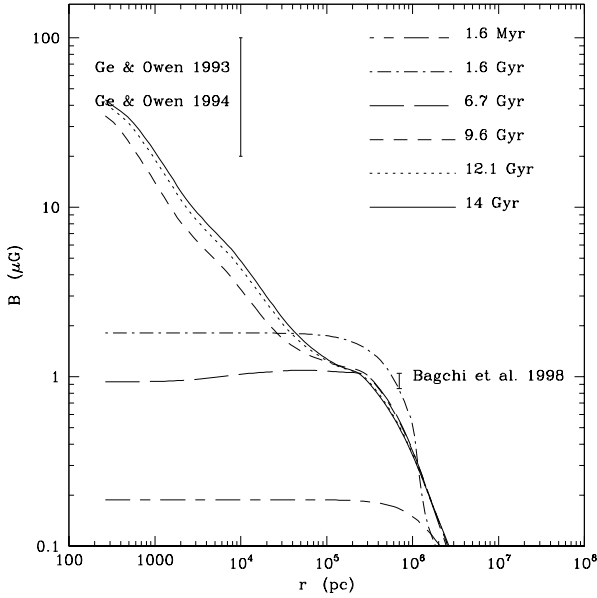


Figure 4. Evolution of the magnetic strength profiles compared to observations. Curves represent early and late stages of the ICM evolution, as labeled, for model II ($\rho_0 = 1.5 \times 10^{-28} \text{ g cm}^{-3}$; $\beta_0 = 10^{-3}$). See the comments on the evolution of B made in the caption of Figure 3.

plification (Eilek 1990; Mathews & Brighenti 1997). However, these processes can not account for the strong magnetic fields observed in the center regions, confirming the expectations previously discussed by authors like Goldshmidt & Rephaeli (1993) and Carvalho (1994).

4 DISCUSSIONS AND CONCLUSIONS

The present models are in many aspects similar to the one of Soker & Sarazin (1990). However there are two important differences between our model and theirs: i) they take into account only small-scale magnetic field effects; and ii) they consider homogenous cooling flow. Since we consider inhomogeneous cooling flow (i.e. \dot{M} decreases with decreasing r) the amplification of B is smaller in our models. As a matter of fact the magnetic pressure reaches equipartition only at radius as small as $\gtrsim 1$ kpc (model I) or $\gtrsim 0.5$ kpc (model II), because the central increase of the β ratio is moderate in our model. Our more realistic description of the field geometry is crucial. This implies that the effect of the magnetic pressure on the total pressure of the intracluster medium, even on regions as inner as few kpc, is small. Tribble (1993) studying the formation of radio haloes in cooling flow clusters from the point of view of the cluster evolution via mergers, suggested typical magnetic field strengths of $\sim 1 \mu\text{G}$. In addition, Zoabi et al. (1996), studying a completely different characteristic of the ICM (magnetic fields on the support of X-rays clumps and filaments), adopted the usually assumed magnetic to pressure ratio, at few scales of 10 – 20 kpc, of 0.1, and following a simple geometry of the field in which it is amplified by the radial inflow, this ratio become ~ 1 at

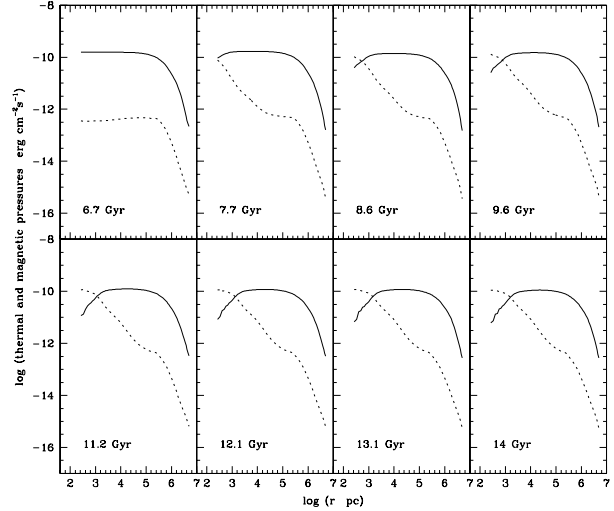


Figure 5. Evolution of the magnetic (dashed lines) and thermal (full lines) pressure profiles on late stages of the ICM evolution for model I. Noting that the magnetic pressure increases until reaches equipartition at inner regions of the cooling flow (at scales $\gtrsim 1$ kpc).

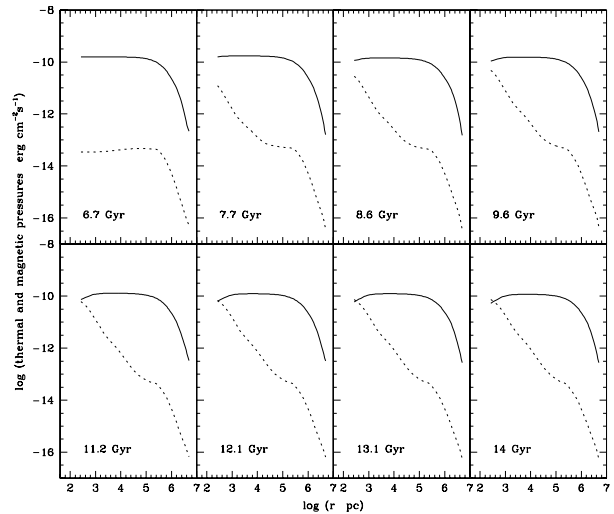


Figure 6. Evolution of the magnetic (dashed lines) and thermal (full lines) pressure profiles on late stages of the ICM evolution for model II. Noting that the magnetic pressure increases until reaches equipartition at inner regions of the cooling flow (at scales $\gtrsim 0.5$ kpc).

~ 5 kpc. Again our results are more or less compatible with the above ones (for the cluster scale magnetic field), but the equipartition condition is reached at smaller scales.

There are a number of papers discussing heating processes on the inner part of the cooling flow clusters, in particular mechanisms to power the emission lines of optical filaments, which use the magnetic energy transformed in optical emission via magnetic reconnection (Jafelice & Friaça

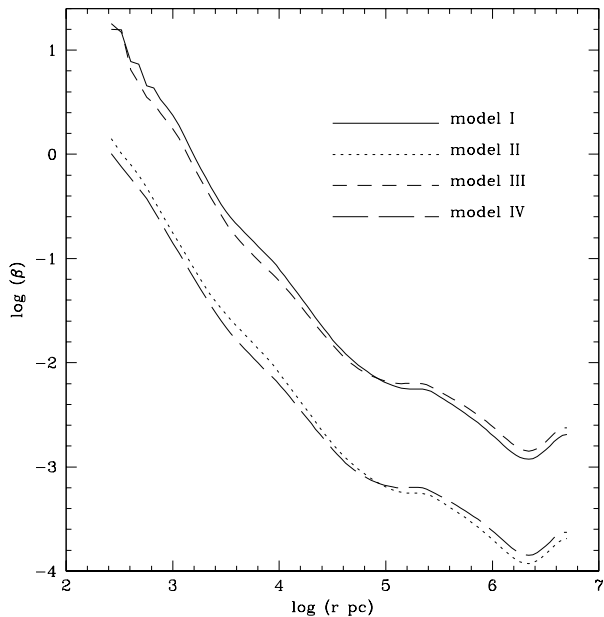


Figure 7. β profiles on 14 Gyr for models I - IV. The profiles are quite similar, except for the fact that models with $\beta_0 = 10^{-3}$ have final β -values lower. From the figure is also clear that the equipartition condition occurs at outer radii for higher β_0 models, and that anyway this condition is reached only on radii smaller than ~ 1 kpc.

1996) or dissipation of Alfvén waves (Friaça et al. 1997). These works are based in the enhancement of the magnetic pressure on scales smaller than ~ 10 kpc, where the filaments are observed (Heckman et al. 1989). Finally, our results suggest that the effect of the magnetic fields on the ICM dynamics can be relevant only on very small scales: $\beta \sim 10^{-1}$, $r \lesssim 10$ kpc, and $\beta \sim 1$, $r \lesssim 1$ kpc, depending on the model adopted (see Figure 7). From Figure 7 one can see quite clearly that the equipartition condition is reached at smaller radii for models in which β_0 is equal to 10^{-3} (model II and model IV), emphasizing the agreement between our models, another theoretical models, and observations.

It is also quite relevant noting that the general agreement of our models and the available data can be emphasized by the fact that observations give us only limits on the magnetic field intensities. In the case of rotation measures the limit is the upper one, in contrast with the data coming from inverse Compton scattering which give the lower limit of this quantity. Therefore, from our best model (model I, see Figure 3) the expected field intensity is lower than the observed value (provided via rotation measures), on scales of 10 kpc, and higher than the field intensity derived from X-ray inverse Compton scattering, on larger scales (700 kpc).

That the discrepancy found in the determination of mass, from gravitational lensing and from X-rays observations (Loeb & Mao, 1994; Loewenstein, 1994; Miralda-Escudé & Babul, 1995), and in the mass distribution of the gravitating matter, mostly dark matter (Eyles et al. 1991), can be consequences of the standard description of the ICM, in which it is assumed hydrostatic equilibrium driven by

thermal pressure (Fabian 1994), is a subject of discussion. Allen (1998) argued that, at least for cooling flow clusters, the above discrepancy is resolved and, therefore, the effect of non-thermal pressures on the hydrostatic equilibrium of these systems could be completely discarded. However, it is important to point out that the radius in which magnetic pressure reaches equipartition is much smaller than the core or arc radii obtained by Allen in his analysis (~ 50 kpc, in average), implying that, despite Allen's results, at smaller scales the non-thermal pressures can be important.

Theoretical models, like the one here presented, point out that magnetic pressure does affect the hydrostatic equilibrium of the ICM, but only in the inner radius, as small as ~ 1 kpc. In addition, it is important to remind that there are other sources of non-thermal pressures that could be considered jointly to the magnetic pressure before to close the discussion on whether or not non-thermal pressures can explain the discrepancies on the mass estimations of the galaxy clusters.

Acknowledgements

One of the authors (D.R.G.) would like to thank the Brazilian agency FAPESP (97/05246-3) for support, and the other author (A.C.S.F.) would like to thank the Brazilian agency CNPq for partial support. We also would like to acknowledge partial support by Pronex/FINEP (41.96.0908.00).

REFERENCES

- Allen S.W., 1998, MNRAS, 296, 392
 Allen S.W., Fabian A.C., 1994, MNRAS, 269, 409
 Bagchi J., Pislár V., Lima Neto G.B., 1998, MNRAS, 296, L23
 Carvalho J.C., 1994, A&A, 281, 641
 Cloutman L.D., 1980, Los Alamos Report, LA - 8452 - MS
 David L.P., Bregman J.N., 1989, ApJ, 337, 97
 Edge A.C., Stewart A.C., 1991, MNRAS, 252, 414
 Eilek J., 1990, in Clusters of Galaxies, ed. M.J. Fitchett, W.R. Oegerle, & L. Danly (Baltimore: STScI), 59
 Ensslin T.A., Biermann P.L., 1998, A&A, 330, 90
 Ensslin T.A., Biermann P.L., Kronberg P.P., Wu X.-P., 1997, ApJ, 477, 560
 Eyles et al., 1991, ApJ, 376, 23
 Fabian A.C., 1994, ARA&A, 32, 277
 Feretti L., Dallascasa D., Giovannini G., Tagliana A., 1995, A&A, 302, 680
 Fort B., Mellier Y., 1994, A&AR, 5, 239
 Friaça A.C.S., 1986, A&A, 164, 6
 Friaça A.C.S., 1993, A&A, 269, 145
 Friaça A.C.S., Gonçalves D.R., Jafelice L.C., Jatenco-Pereira V., Opher R., 1997, A&A, 324, 449
 Ge J.P., Owen F.N., 1993, AJ, 105, 778
 Ge J.P., Owen F.N., 1994, AJ, 108, 1523
 Godon P., Soker, N., & White III, R.E. 1998, AJ, 116, 37
 Goldshmidt O., & Rephaeli Y., 1993, ApJ, 411, 518
 Grevesse N., Anders E., 1989, in Waddington C.J., ed., Cosmic Abundances of Matter. AIP, New York, p.183
 Gruenwald R.B., Viegas S.M., 1992, ApJS, 78, 153
 Heckman T.M., Baum S.A., Van Breugel W.J.M., McCarthy P., 1989, ApJ, 338, 48
 Jafelice L.C., Friaça A.C.S., 1996, MNRAS, 280, 438
 Kim J.P., Butcher J.A., Stewart G.C., Tanaka Y., 1990, ApJ, 335, 29
 Lieu R. et al. 1996, Science, 274, 1335

- Loeb A., Mao S., 1994, *ApJ*, 435, L109
Loewenstein M., 1994, *ApJ*, 431, 91
Mathews W.G., Brighenti F., 1997, *ApJ*, 488, 595
Miralda-Escudé J., Babul A., 1995, *ApJ*, 449, 18
Nulsen P.E.J., Böhringer H., 1995, *MNRAS*, 274, 1093
Peres C.B., et al., 1998, *MNRAS*, 298, 416
Pistinner S., Levinson A., Eichler D., 1996, *ApJ*, 467, 162
Rephaeli Y., Gruber D.E., 1988, *ApJ*, 333, 133
Rephaeli Y., Gruber D.E., Rothschild R.E., 1987, *ApJ*, 320, 139
Ryu D., Biermann P.L., 1998, *A&A*, 335, 19
Smail I., Ellis R.E., Dressler A., Couch W.J., Oemler A., Sharples R.M., Butcher H., 1997, *ApJ*, 479, 70
Sarazin C.L., 1992, in “Clusters and Superclusters of Galaxies”, ed. A.C. Fabian, NATO ASI Series, p. 131
Soker N., Sarazin C.L., 1990, *ApJ*, 348, 73
Sreekumar et al., 1996, *ApJ*, 464, 628
Taylor G.B., Perley R.A., 1993, *ApJ*, 416, 554
Tribble P.C., 1993, *MNRAS*, 263, 31
Tscharnutter W.M., Winkler K.H., 1979, *Comp. Phys. Comm.*, 18, 171
White III R.E., Sarazin C.L., 1987, *ApJ*, 318, 612
Wu X.P., Fang L.Z., 1996, *ApJ*, 467, L45
Wu X.P., Fang L.Z., 1997, *ApJ*, 483, 62
Wu X.P., Chieuh T., Fang L.Z., Xue Y.J., 1998, *MNRAS*, 301, 861
Zoabi E., Soker N., Reveg O., 1996, *ApJ*, 460, 244